5-30-2006

Microswitches with Sputtered Au, AuPd,Au-on-AuPt, and AuPtCu Alloy Electric Contacts

Ronald A. Coutu Jr.
Marquette University, ronald.coutu@marquette.edu

J. R. Reid
Air Force Research Laboratory

R. Cortez
Air Force Research Laboratory

R. E. Strawser
Air Force Research Laboratory

P. E. Kladitis
Air Force Institute of Technology

Accepted version. *IEEE Transactions on Components and Packaging Technologies*, Vol. 29, No. 2, (June 2006): 341-349. DOI.
R.A Coutu was affiliated with the Antenna Technology Branch, Air Force Research Laboratory, Hanscom Air Force Base, MA at the time of publication.

Contents

Microswitches with Sputtered Au, AuPd,Au-on-AuPt, and AuPtCu Alloy Electric Contacts

Ronald A. Coutu
Antenna Technology Branch, Air Force Research Lab, Hanscom, MA
J. R. Reid
Antenna Technology Branch, Air Force Research Lab, Hanscom, MA
R. Cortez
Air Force Research Laboratory, Wright-Patterson AFB, OH
R. E. Strawser
Air Force Research Laboratory, Wright-Patterson AFB, OH
P. E. Kladitis
Department of Electrical and Computer Engineering, Air Force Technology Institute, Wright Patterson AFB, OH

Abstract:

This paper is the first to report on a new analytic model for predicting microcontact resistance and the design, fabrication, and testing of microelectromechanical systems (MEMS) metal contact switches with sputtered bimetallic (i.e., gold (Au)-on-Au-platinum (Pt), (Au-on-Au-(6.3at%)Pt)), binary alloy (i.e., Au-palladium (Pd), (Au-(3.7at%)Pd)), and ternary alloy (i.e., Au-Pt-copper (Cu), (Au-(5.0at%)Pt-(0.5at%)Cu)) electric contacts. The microswitches with bimetallic and binary alloy contacts resulted in contact resistance values between 1-2Omega. Preliminary reliability testing indicates a 3times increase in switching lifetime when compared to microswitches with sputtered Au electric contacts. The ternary alloy exhibited approximately a 6times increase in switch lifetime with contact resistance values ranging from approximately 0.2-1.8Omega

SECTION I. Introduction

Microelectromechanical systems (MEMS) switches are paramount in importance for the future miniaturization of radio frequency (RF) systems. Space-based radar, phased array radar, and phase shifters all depend on reliable switching between RF loads. Because of their small geometries, exceptional RF performance, and low power consumption, MEMS contact switches are ideally suited for these applications.[1] The devices used in this study are illustrated in Fig. 1.

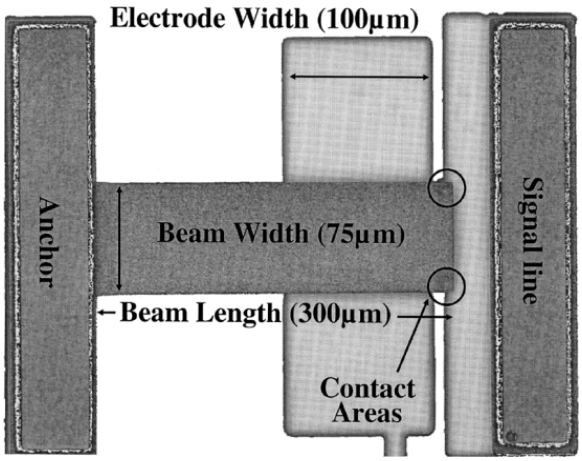

Fig. 1. Captured video image of a cantilever-style microswitch.

Important performance criteria for microswitch applications are low contact resistance ($\sim 1-2\Omega$) and reliability ($> 10^8$ "hot-switched" switch cycles). The two primary failure mechanisms for MEMS metal contact switches are becoming stuck closed (i.e., stiction) and increased contact resistance with increasing switch cycles. Typically, microswitches use gold-on-gold (Au) electric contacts to achieve low contact resistance due to gold's low resistivity and low susceptibility to oxidation. MEMS switches with Au electric contacts, however, are prone to stiction and low reliability due to Au's relative low hardness (i.e., Meyer hardness between $\sim$ 1–2GPa). The purpose of this work is to develop an analytic model for predicting microcontact resistance and also to fabricate microswitches optimized for increased reliability with relatively low contact resistance.

When modeling microcontact resistance, neglecting ballistic electron transport[2] and contaminant film resistance[3] underestimates contact resistance for low contact force applications. Majumder et al. considered ballistic and diffusive electron transport using Wexler's interpolation[4] and considered contact material deformation using Hertz's elastic[5] and Chang et al.'s elastic-plastic[6] (i.e., the Chang, Etison, and Bogy or the CEB model) models.[3] Majumder et al.'s contact resistance model, however, uses Wexler's original Gamma function derivation and does not account for the contact load discontinuity found in the CEB model.

Kogut and Komvopoulos derived an electrical contact resistance (ECR) model for conductive rough surfaces based on a fractal geometry surface topography description, elastic-plastic deformation of contacting asperities, and size-dependent electrical constriction resistance of microcontacts comprising the real contact area.[7] Additional work by Kogut and Komvopoulos resulted in an ECR model for conductive rough surfaces coated with a thin insulating layer based fractal geometry to describe the surface topography, elastic, elastic-plastic, and fully plastic deformation of surface asperities, and quantum mechanics considerations for the electric-tunnel effect through a thin insulating layer.[8] Kogut and Komvopoulos used Mikrajuddin et al.'s[10] derived Gamma function in Wexler's interpolation[4] to account for size-dependent constriction resistance. In addition, the Kogut and Komvopoulos ECR models, as well as Majumder et al.'s model, are based on the assumption that contacting surface asperities have sufficient separation and are independent.

In this work, the independent surface asperity assumption is no longer valid due to the properties of the sputtered electric contact films used (addressed in more detail later). An updated microcontact resistance model is developed using Chang's[9] improvements to the CEB model[6] and Mikrajuddin et al.'s[10] Gamma function in Wexler's interpolation.[4] Last, contaminant film resistance is briefly investigated using measured contact resistance data.

In addition, previous microswitch work has focused on optimizing the mechanical aspects of microswitch designs rather than investigating different contact metals.[11] Notable exceptions are Majumder et al.'s and Duffy et al.'s utilization of a "platinum group" and Pt contact metals, respectively.[12,13] These metals were chosen over Au for their increased hardness and improved wear characteristics. In order to achieve acceptable contact resistance, Majumder et al.'s microswitches required multiple (i.e., 4 to 8), parallel contacts and were packaged in a hermetic environment while Duffy et al.'s MEMS switches required actuation voltages approximately 45V higher than the pull-in voltage. Schimkat studied Au-nickel (Ni) alloy (Au-(5at%)Ni) macroswitch contacts in a low-force test configuration.[14] In this work, MEMS cantilever-style switches were designed, fabricated, and tested with sputtered bi-metallic (i.e., Au-on-Au-platinum (Pt), [Au-on-Au-(6.3at%)Pt)], binary alloy (i.e., Au-palladium (Pd), [Au-(3.7at%)Pd)], and ternary alloy (i.e., Au-Pt-copper (Cu), [Au-(5.0at%)Pt-(0.5at%)Cu)] contact metals and hemispherical-shaped upper and planar lower contact geometries.

Generally, microswitches with Au electric contacts exhibit approximately 10^6 "hot-switched" cycles because evaporated Au is a soft metal and prone to erosion.[12,15] Zavracky et al. report $5 \cdot 10^8$ "hot-switched" cycles and over $2 \cdot 10^9$ "cold-switched" cycles for microswitches with Au sputtered contacts that were packaged in nitrogen.[15] Majumder et al. reports greater than 10^7 "hot-switched" cycles and approximately 10^{11} "cold-switched" cycles for microswitches with a "platinum group" contact metal.[12] In this work, test results for microswitches with bi-metallic, binary alloy, and ternary alloy contact metals are presented.

SECTION II. Contact Resistance Modeling

An understanding of contact mechanics is needed to design microsized electric contacts and predict contact resistance. There are two primary considerations: 1) how the contact material deforms (elastic, plastic, or elastic-plastic) and 2) the radius of the effective contact area.

A. Material Deformation Models

1) Elastic

When two surfaces are initially pressed together, with low contact force, surface asperities (i.e., a-spots) undergo elastic deformation. Equations (1) and (2) define the contact area and force as a function of vertical deformation for a single a-spot[9]

$$A = \pi R \alpha \quad (1)$$

where A is contact area, R is asperity peak radius of curvature, and α is asperity vertical deformation

$$F_{cE} = \frac{4}{3} E' \alpha \sqrt{R\alpha} \quad (2)$$

where F_{cE} is the normal contact force and E' is the Hertzian modulus derived from

$$\frac{1}{E'} = \frac{1-v_1^2}{E_1} - \frac{1-v_2^2}{E_2} \text{ (3)}$$

where E_1 is the elastic modulus for contact one, v_1 is Poisson's ratio for contact one, E_2 is the elastic modulus for contact two, and v_2 is Poisson's ratio for contact two.

For circular areas (i.e., $A = \pi r^2$), (1) and (2) are related to the contact area radius (r) through Hertz's model[5]

$$r = \sqrt[3]{\frac{3F_{cE}R}{4E'}}. \text{ (4)}$$

When the applied load increases to approximately three times the yield stress (σ_Y) or yield point (Y), material deformation is no longer reversible and ideal plastic material deformation begins.[5]

2) Plastic

Plastic material deformation is modeled using Abbott and Firestone's well-known model that assumes sufficiently large contact pressure and no material creep.[16] Single asperity contact area and force are defined using (5) and (6):

$$A = 2\pi R\alpha \text{ (5)}$$

$$F_{cP} = HA \text{ (6)}$$

where H is the Meyer hardness of the softer material.[9]

Using (6), circular contact area radius is related to contact force through (7)[5]

$$r = \sqrt{\frac{F_{cP}}{H\pi}}. \text{ (7)}$$

An area discontinuity exists when transitioning from ideal elastic to ideal plastic behavior when the elastic model from Section II-A and this plastic model are used together.[5] The CEB model, discussed next, addresses this issue by assuming volume conservation of deformed surface asperities.[6]

3) Elastic-Plastic

Elastic-plastic material deformation refers to when parts of the contact area are plastically deforming but are encased by elastically deformed material.[17] The Chang, Etison, and Bogy or CEB elastic-plastic model describes material deformation that occurs between the ideal elastic and ideal plastic regions.[6]

Equations (8) and (11) are the CEB model's contact area and force equations, respectively[6]

$$A = \pi R\alpha\left(2 - \frac{\alpha_c}{\alpha}\right) \text{ (8)}$$

where α_c is critical vertical deformation, where elastic-plastic behavior begins, given as

$$\alpha_{\mathrm{c}} = R\left(\frac{K_{\mathrm{H}} H\pi}{2E'}\right)^2 \text{ (9)}$$

where K_{H} is the hardness coefficient (assumed to be 0.6 at the onset of plasticity[6]) given as

$$K_{\mathrm{H}} = 0.454 + 0.41\nu \text{ (10)}$$

where ν is Poisson's ratio

$$F_{\mathrm{cEP}} = K_{\mathrm{H}} HA. \text{ (11)}$$

In the CEB model, a contact load discontinuity exists at the transition from elastic to elastic–plastic material deformation. Kogut and Etison addressed this using finite element methods to model the elastic-plastic region with normalized contact force and area equations based on Hertzian elastic contact mechanics.[18] Chang observed that ideal plastic behavior normally occurred at $3Y$, not $K_{\mathrm{Y}}Y$ (i.e., K_{Y} is the yield coefficient) and updated the CEB model with a linear interpolation.[9] Chang's new force equation for elastic-plastic material deformation is given by

$$F_{\mathrm{cEP}} = \left[3 + \left(\frac{2}{3}K_Y - 3\right)\frac{\alpha_c}{\alpha}\right] YA \text{ (12)}$$

where $K_{\mathrm{Y}} = 1.1282 + 1.158\nu$.[9]

The yield strength for most metals is related to its hardness through (13)[9]

$$Y = 0.354H. \text{ (13)}$$

When K_{Y} and (13) are substituted into (12), Equation (14) results in

$$F_{\mathrm{cEP}} = \left[1.062 + 0.354\left(\frac{2}{3}K_Y - \left(3\frac{\alpha_c}{\alpha}\right)\right)\right] HA. \text{ (14)}$$

Equations (8) and (14) represent the CEB model[6] updated with Chang's improvements.[9]

For circular areas, (14) is used to relate the contact area radius and the contact force through

$$r = \sqrt{\frac{F_{\mathrm{cEP}}}{H\pi\left[1.062+0.354\left(\frac{2}{3}K_Y-3\left(\frac{\alpha_c}{\alpha}\right)\right)\right]}}. \text{ (15)}$$

The contact area radius, determined from material deformation models, is a function of the contact force generated by the microswitch.

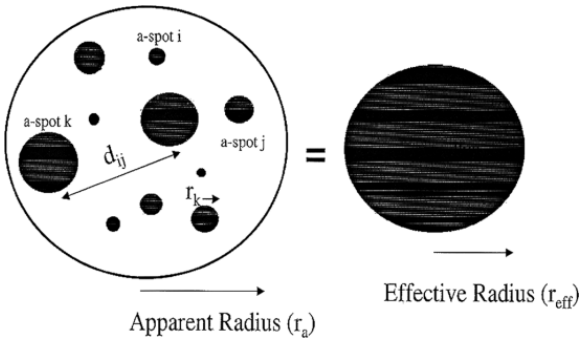

Fig. 2. Top view of the (a) multiple asperity and (b) single effective asperity contact area models.

B. Contact Force and Area

Contact force is a compressive force that causes material deformation by bulging.[17] Generally, MEMS switches are electrostatic devices that produce low contact forces ranging from tens of μN 's up to a few mN 's.

In microswitches, contact force is defined by the mechanical switch design while contact area is defined by contact geometry, surface roughness, elastic modulus, and material hardness. From this description two contact area models have been developed: 1) the multiple a-spot and 2) the single effective a-spot.

The multiple asperity model is based on Greenwood and Williamson's “asperity-based model” for elastic material deformation and Abbott and Firestone's “profilometric model” for plastic deformation.[16,19]

The assumptions used by Greenwood and Williamson follow: 1) contact surfaces are isotropic with known surface roughness, 2) all surface asperity peaks are spherical with the same radii of curvature, 3) asperity height is randomly distributed, 4) asperities are far apart and independent, 5) material deformation occurs only in the asperities, and 6) no heating occurs. McCool studied anisotropic rough surfaces with randomly distributed elliptically asperities which revealed exceptional agreement with Greenwood and Williamson's simpler model.[20] Greenwood and Tripp showed that two rough contacting surfaces could be modeled by an equivalent single rough surface contacting a flat, smooth surface.[21]

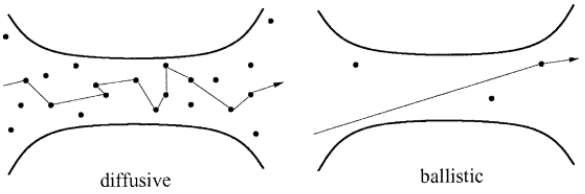

Fig. 3. Schematic illustration of (a) diffusive and (b) ballistic electron transport in a conductor.[22]

In the single effective asperity model, the individual contact spots are close enough together that their interactions are not independent. In this situation, the effective contact area is defined as the sum, not the parallel combination, of the individual contact areas. Fig. 2 illustrates the multiple a-spot and single effective a-spot models and the notion of an effective contact area radius (r_{eff}).

Majumder et al. predicted a lower contact resistance bound when using the multiasperity model and an upper contact resistance bound when using the single effective a-spot model.[3]

The contact area radius determines how conducting electrons are transported through individual electrical connections. A brief discussion about the resistance resulting from ballistic, quasiballistic, and diffusive electron transport follows.

C. Contact Resistance and Electron Transport

Contact resistance (R_{C}), defined by (16), results from making electrical connections and considers the effects of constriction (R_{C}) and contaminant film (R_{cf}) resistances:[5]

$$R_C = R_c + R_{\mathrm{cf}}. \quad (16)$$

Constriction resistance arises because electrical current can only flow through conducting a-spots created after switch closure. Constriction resistance, based on diffusive electron transport and Maxwellian spreading resistance theory, is modeled analytically using (17)[5]

$$R_{c\mathrm{D}} = \frac{p}{2r_{\mathrm{eff}}} \quad (17)$$

where $R_{c\mathrm{D}}$ is constriction resistance and ρ is resistivity.[5] Constriction resistance is equal to contact resistance when contaminant film resistance is neglected.

When considering circular contact areas, (18) and (19) are the resulting macroswitch contact resistance equations for elastic material deformation (i.e., $R_{\mathrm{c}} \propto F_{\mathrm{c}}^{(-1/3)}$) and plastic deformation (i.e., $R_{\mathrm{c}} \propto F_{\mathrm{c}}^{(-1/2)}$)[5]

$$R_{c\mathrm{DE}} = \frac{p}{2}\sqrt[3]{\frac{4E'}{3F_cR}} \quad (18)$$

where R_{cDE} is contact resistance for diffusive transport and elastic deformation and

$$R_{c\mathrm{DP}} = \frac{p}{2}\sqrt{\frac{H\pi}{F_c}} \quad (19)$$

where R_{cDP} is contact resistance for diffusive transport and plastic deformation.

Microswitches produce much lower contact force than macroswitches resulting in smaller contact areas. When the contact area radius is compared to an electron's elastic mean free path (l_{e}), the following electron transport regions are defined: ballistic (i.e., $l_{\mathrm{e}} > r_{\mathrm{eff}}$), quasiballistic (i.e., $l_{\mathrm{e}} \sim r_{\mathrm{eff}}$), and diffusive (i.e., $l_{\mathrm{e}} \ll r_{\mathrm{eff}}$).[3,22] The mean free path for most metals is approximately 500rmAA.[22] Fig. 3 illustrates the ballistic and diffusive electron transport regions.[22]

Equation (20) or the Sharvin resistance is a semiclassical approximation for contact resistance when ballistic electron transport dominates[22]

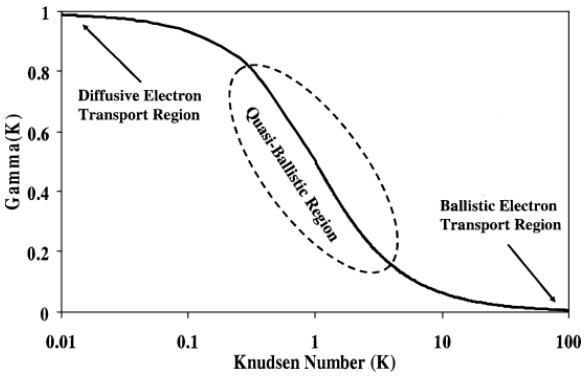

Fig. 4. Plot of Mikrajuddin et al.'s derived Gamma function.

$$R_{\mathrm{cB}} = \frac{4\rho K}{3\pi r_{\mathrm{eff}}} \quad (20)$$

where R_{cB} is the Sharvin resistance and K is the Knudsen number given as

$$K = \frac{l_e}{r_{\mathrm{eff}}}. \quad (21)$$

Wexler derived (22) to interpolate between the ballistic and diffusive electron transport regions[4]

$$\begin{aligned} R_{\mathrm{W}} = & \quad \frac{4\rho K}{3\pi r_{\mathrm{eff}}}\left[1 + \frac{3\pi}{8}\Gamma(K)\frac{r_{\mathrm{eff}}}{l_{\mathrm{e}}}\right] \quad (22) \\ = & \quad R_{\mathrm{cB}} + \Gamma(K)R_{\mathrm{cD}} \end{aligned}$$

where R_W is the Wexler resistance and $\Gamma(K)$ is a slowly varying Gamma function of unity order.[4]

D. New Microcontact Resistance Model

An updated analytic microcontact resistance model, based on the single effective a-spot contact area model, is developed using Hertz's elastic,[5] Chang's[9] improvements to the CEB model, Wexler's interpolation from ballistic to diffusive electron transport,[4] and Mikrajuddin et al.'s Gamma function.[10]

The single effective a-spot contact area model is needed because independent conducting surface asperities can no longer be assumed. The sputtered contact films used here exhibited low measured surface roughness (i.e., ≈30–50 AA) and tightly packed material grain structures (i.e., ≈50nm in diameter). In addition, the microswitch's actual contact geometries (i.e., hemispherical-shaped upper and planar lower) closely match the analytic elastic and elastic-plastic material deformation models presented earlier.

Mikrajuddin et al.'s Gamma function,

$$\Gamma(K) \approx \frac{2}{\pi}\int_0^{\infty} e^{-Kx} Sinc(x)\mathrm{d}x \quad (23)$$

where Sinc(x) is defined as being equal to one when $x = 0$ and equal to $Sin(x)/x$ when $x \neq 0$,[10] was solved using a recursive Newton–Cotes numerical integration formula and plotted in Fig. 4.

For circular contact areas and elastic material deformation, a contact resistance equation is derived for the ballistic electron transport region by substituting (4) into (20) resulting in

$$R_{cBE} = \frac{4pK}{3\pi}\sqrt[3]{\frac{4E'}{3F_cR}} \quad (24)$$

where R_{cBE} is the contact resistance for ballistic electron transport and elastic deformation.

Equation (25), the new microcontact resistance model for elastic deformation, results when (24) and (18) are substituted into (22)

$$R_{\mathrm{WE}} = R_{\mathrm{cBE}} + \Gamma(K)R_{\mathrm{cDE}} \quad (25)$$

where R_{WE} is the Wexler resistance for elastic material deformation.

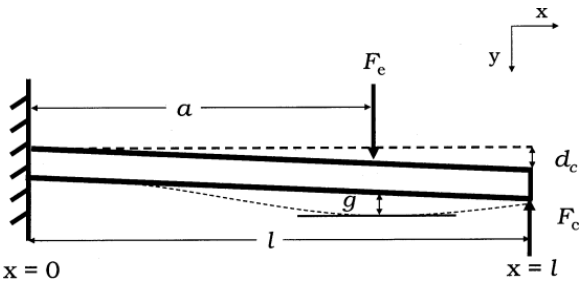

Fig. 5. Cantilever beam model with a fixed end at $x = 0$, a simply supported end at $x = l$, and an intermediately placed load (F_{c}) at $x = a$.

Equation (26) is a contact resistance equation based on ballistic electron transport and elastic–plastic material deformation and is found by substituting (15) into (20)

$$R_{\mathrm{cBEP}} = \frac{4\rho K}{3\pi}\sqrt{\frac{H\pi\left[1.062+0.354\left(\frac{2}{3}K_{\mathrm{Y}}-3\left(\frac{\alpha_c}{\alpha}\right)\right)\right]}{F_{\mathrm{c}}}}. \quad (26)$$

Equation (27) is a contact resistance equation based on diffusive electron transport and elastic–plastic material deformation and is found by substituting (15) into (17)

$$R_{\mathrm{cDEP}} = \frac{\rho}{2}\sqrt{\frac{H\pi\left[1.062+0.354\left(\frac{2}{3}K_{\mathrm{Y}}-3\left(\frac{\alpha_c}{\alpha}\right)\right)\right]}{F_{\mathrm{c}}}}. \quad (27)$$

Equation (28), the new microcontact resistance model for elastic-plastic deformation, results when (26) and (27) are substituted into (22)

$$R_{\mathrm{WEP}} = R_{\mathrm{cBEP}} + \Gamma(K)R_{\mathrm{cDEP}} \quad (28)$$

where R_{WEP} is the Wexler resistance for elastic-plastic material deformation.

SECTION III. MEMS Switches

A brief discussion of the design, fabrication, and testing of the microswitches in this study, shown in Fig. 1, is presented next.

A. Design

In metal contact microswitches, initial switch closure is defined by the pull-in voltage. At pull-in physical contact between the upper (i.e., dimples) and lower contacts is first established with minimal contact force. As the actuation voltage is increased, contact force also increases and material deformation causes the contact area to increase. After pull-in, the microswitch is modeled as a deflected beam with a fixed end, a simply supported end, and an intermediately placed load as illustrated in Fig. 5.

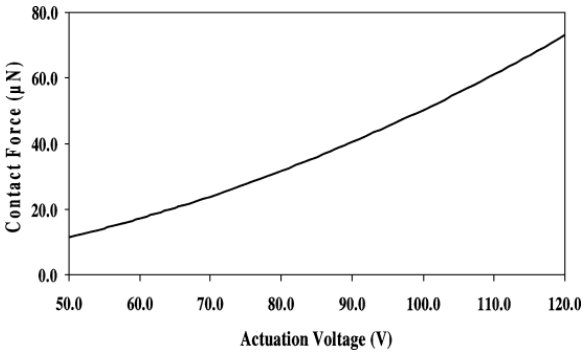

Fig. 6. Microswitch contact force (per contact) plot.

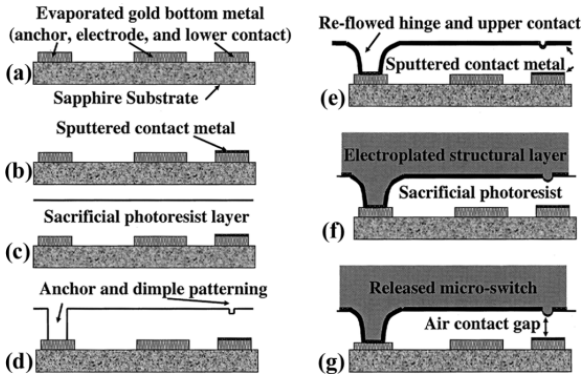

Fig. 7. Illustration of the microswitch fabrication process.

Using a parallel plate capacitor model and neglecting fringing fields, the intermediately placed load is modeled as

$$F_{\mathrm{e}} = \frac{\epsilon_{\mathrm{o}} A_{\mathrm{sa}} V^2}{2g^2} \quad (29)$$

where F_e is the electrostatic force, $\in_0$ is the permittivity of free space, A_{sa} is the surface area of the smaller parallel plate, V is the actuation voltage, and g is the gap between the plates.[23]

Equation (30) is the resulting contact force equation

$$F_c = \left[\frac{F_e a^2}{2l^3}(3l - a) - \frac{EI_z d_c}{l^3}\right] \quad (30)$$

where F_c is contact force, a is the location of the electrostatic force, l is beam length, d_c is beam tip deflection distance, and I_z is the area moment of inertia about the z -axis defined by

$$I_z = \frac{wt^3}{12} \quad (31)$$

where w is the beam width and t is the beam thickness.[24]

Microswitch contact force, illustrated by Fig. 6, is mapped to actuation voltage using (30).

After completing the microswitch mechanical design, using (29)–(31), a compatible thin film deposition process (i.e., cosputtering) was chosen and candidate electric contact metal alloys were selected.

B. Fabrication

The microswitches in this study were fabricated on highly resistive sapphire substrates. Four wafers of devices, each with a different contact metallurgy (i.e., sputtered Au, Au-on-Au-(6.3at%)Pt, Au-(3.7at%)Pd, and Au-(5.0at%)Pt-(0.5at%)Cu) were individually fabricated using the process illustrated in Fig. 7. Refer to Fig. 7 for the following discussion.

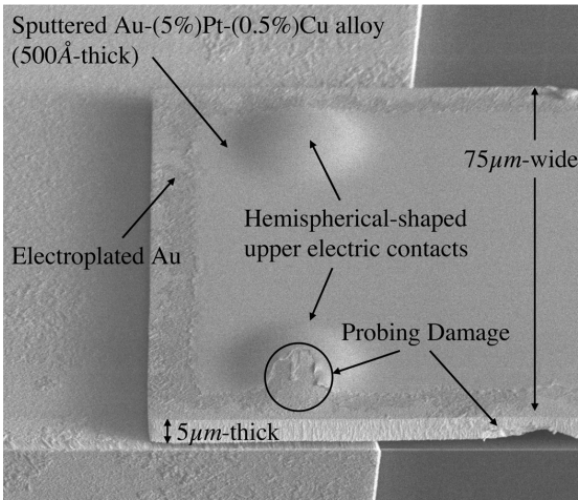

Fig. 8. Scanning electron micrograph (SEM) image showing the hemispherical-shaped upper contacts and the sputtered electric contact metal. Probing damage occurred while flipping the cantilever beam for imaging.

The actuation electrode and lower electric contact layers were formed using a standard lift-off process with 3000AA of evaporated Au and a 200AA of chromium (Cr) adhesion layer (a).[25] The lower electric contact metal was sputter deposited (500AA-thick) and patterned using a metal lift-off technique (b).

The beam's gap or sacrificial layer was approximately 3-μ m-thick and was created using MicroChem's polydimethylglutarimide (PMGI) based photoresist (c).[26] The microswitch's hinge geometry was defined in the sacrificial photoresist using standard photolithography techniques while the upper contact geometries were defined by a partial expose and develop of the sacrificial photoresist layer (d). A timed reflow in an oven with flowing nitrogen was used to reform the dimple into a hemispherical-shaped upper contact bump (e).

The upper contact metals were also sputter deposited (500AA-thick), and patterned using standard photolithography techniques (e). The upper contact material, located on the underside of the cantilever beam, is highlighted in Fig. 8.[27]

The structural layer consisted of electroplated Au approximately 55 μ m-thick (f). The devices were released using a CO_2 critical point dryer and tested to ensure proper operation and performance (g).

C. Test Results

A series of 20 microswitches were tested on four different wafers (80 switches total) to experimentally characterize contact resistance. Microswitch lifetime data, from selected devices with alloy electric contacts, were collected and compared to microswitches with sputtered Au contacts. The experimental setup, illustrated in Fig. 9, was used for both tests.

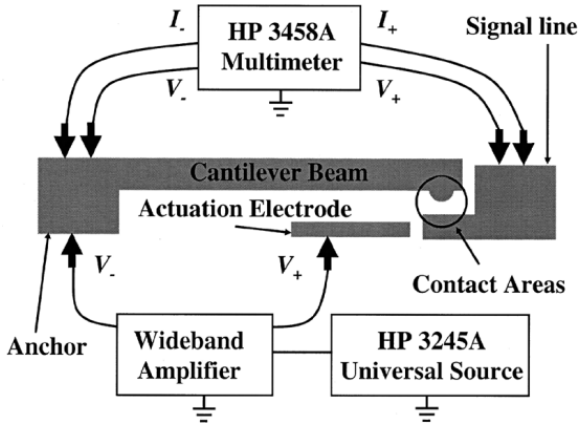

Fig. 9. Experimental test setup used to measure pull-in voltage, contact resistance, and switch lifetime.

TABLE I Average Minimum Contact Resistance (R_c) and Standard Deviation for Measured Data. Simulated R_c was Found Using Measured Material Properties and (28)

Metal/Alloy	R_c (Ω) / StdDev Experiment 1	R_c (Ω) / StdDev Experiment 2	R_c (Ω) Simulated
Au	0.94 / 0.20	0.83 / 0.19	0.10
Au-(3.7at%)Pd	1.23 / 0.19	1.17 / 0.07	0.17
Au-on-Au-(6.3at%)Pt	1.13 / 0.13	0.99 / 0.16	0.14
Au-(5.0at%)Pt-(0.5at%)Cu	0.34 / 0.33	0.33 / 0.30	0.20

The microswitches were tested by wafer probing using an Alessi Rel-4100A microprobe station with standard microprobes. The actuation voltage was applied using an HP 3245A universal source and a Krohn–Hite wideband amplifier. Closed switch resistance was measured using an HP 3458A multimeter in a four-point probe configuration. Contact resistance was found by subtracting the measured beam resistance from the closed switch resistance measurements.

During contact resistance testing, a voltage ranging from 0 to 120V in 0.5-V increments was applied between the cantilever beam and the actuation electrode. The microswitch closes when the actuation voltage exceeds the pull-in voltage. As the applied voltage is increased, beyond the pull-in voltage, contact force increases and contact resistance decreases. Contact resistance data were collected each time the actuation voltage was incremented. This test was accomplished twice for each microswitch with approximately 10–15s between the experiments. The average minimum contact resistance data,

with 120V of applied actuation voltage, are summarized in Table I. For comparison, simulated contact resistance values, calculated using measured material properties and (28), are also provided in Table I.

Table I shows that the average minimum contact resistance is somewhat higher than the simulated values. This discrepancy is most likely due, in part, to resistive contaminant film layers on the electric contact's surface.

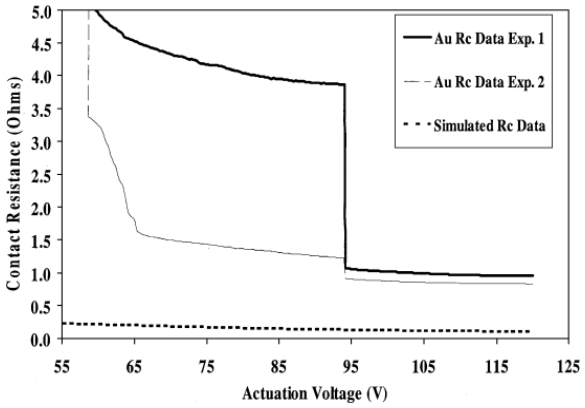

Fig. 10. Contact resistance (R_c) data for a representative microswitch with sputtered Au electric contacts.

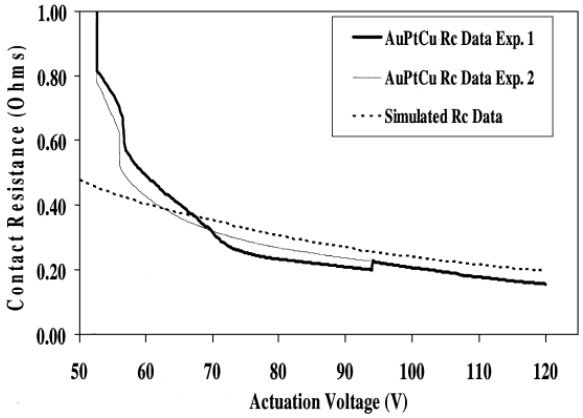

Fig. 11. Contact resistance (R_c) data for a selected microswitch with Au-(5at%)Pt-(0.5at%)Cu electric contacts.

This hypothesis is backed by contact resistance data, collected during experiment two, that is lower than data collected during experiment one.

Measured (using a representative microswitch with Au electric contacts) and simulated (using (25), (28), and measured material properties) contact resistance data are plotted in Fig. 10. The data on Fig. 10 shows a sharp decrease in contact resistance at approximately $\sim$ 93V for microswitches tested the first time. This drop in measured contact resistance was consistent and occurred between 90V and 98V for all the microswitches tested. This anomaly may have been caused by differential electric contact height resulting from the device fabrication process. In other words, one contact touched (i.e., a resistor is series) prior to the decrease and two contacts touched (i.e., two resistors in parallel) after the decrease. In addition, measured contact resistance after the sharp decrease is lower during experiment two than

in experiment one. This result is consistent with data presented in Table I and is most likely due to contaminant film fritting[5] and contact cleaning (i.e., “wiping”). The microswitch contact cleaning mechanism resulted from microswitch beam bending, utilizing hemisphere-shaped electric contacts, and contact region friction.

Fig. 11 shows measured and simulated contact resistance

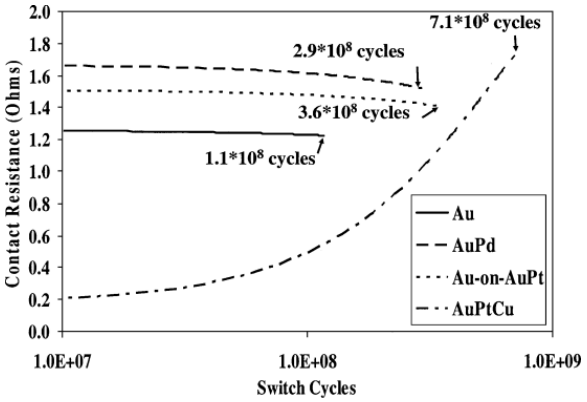

Fig. 12. Contact resistance versus switch cycles data plot.

for microswitches with Au-(5.0at%)Pt-(0.5at%)Cu electric contacts. The measurements, shown on Fig. 11, are somewhat lower than the simulated values. It's possible that the single effective asperity model, used in this study, did not accurately represent the actual contact area for these microswitches. Recall that Majumder et al. showed a contact resistance lower limit using the multiple asperity-based model and an upper limit using the single effective asperity-based mode. This may indicate that the Au-(5.0at%)Pt-(0.5at%)Cu films have larger material grains and higher surface roughness and are better represented using the multiasperity contact area model. More study is needed to verify this hypothesis.

In addition, during experiment one a resistance increase from 0.20 to 0.22Ω was measured at approximately ~ 93V. This small increase in resistance may have been caused by localized contact area heating resulting in a ternary alloy phase change or the formation of an intermetallic compound. This hypothesis is backed by resistance data, collected during the second experiment, that are higher than data from the first experiment (i.e., between 70V and 93V). For actuation voltages higher than ~ 93V the measured resistance values from both experiments agree. This may indicate that the contact material was in a stable state during the second experiment. This anomaly was not observed in the microswitches with binary alloy contacts, most likely, because their alloy compositions avoided miscibility gaps and intermetallic compounds.[28]

During lifecycle testing, the microswitches were actuated using a 50% duty cycle square wave input. The waveform's “on” voltage was set to the pull-in voltage plus approximately 1–3V for increased contact force. The input waveform's frequency was set below the beam's resonant frequency. The microswitches were cycled continuously until they failed open (i.e., infinite resistance) or closed (i.e., stuck down). Contact resistance data were collected every 30s by increasing the input waveform's duty cycle to 90% and lowering its frequency to 1Hz for 2s. The multimeter's open circuit voltage (~8.2V) was present on the contacts for all the switching events (i.e., “hot-switching”). The success criteria for this testing was measured contact resistance less than ~2 Ω and infinite open switch resistance.

Microswitch contact resistance versus switch cycles is plotted on Fig. 12. The raw data was curve fitted with trendlines for selected microswitches with different contact metals.

The microswitches with bi-metallic (Au-on-Au-(6.3at%)Pt) and binary alloy (Au-(3.7at%)Pd) contacts resulted in contact resistance between 1–2Ω. In addition, limited lifecycle data showed that microswitches with sputtered alloy electric contacts, when compared to microswitches with sputtered Au contacts, exhibited approximately a 3× increase in switching lifetime. The microswitches with ternary alloy (Au-(5.0at%)Pt-(0.5at%)Cu) contacts exhibited approximately a 6 times increase in switch lifetime with contact resistance values ranging from 0.2–1.8Ω. The increased lifetimes were most likely due to the increased material hardness of the sputtered metal contact alloys. Also, the microswitches with sputtered Au contacts outperformed other microswitches with Au contacts.[12] Once again, this was most likely due to the increased material hardness of the sputtered Au contact metals. The measured Meyer hardness of evaporated Au, sputtered Au, Au-(2at%)Pd, Au-(6.3at%)Pt, and Au-(5.0at%)Pt-(0.5at%)Cu thin films were approximately 1.0GPa, 1.7GPa, 1.9GPa, 2.0GPa, and 2.2GPa, respectively.

The microswitches with Au-(5.0at%)Pt-(0.5at%)Cu contacts exhibited increased contact resistance with increased numbers of switch cycles. The plot on Fig. 12 shows a steady rise in contact resistance between 10^7 and $7.1 \cdot 10^8$ switch cycles. This is an indication of contact surface evolution and possibly the formation of a polymer-based contaminant film layer (due to “hot-switching”). This hypothesis is supported by the high closed switch resistance failure mechanism observed while testing these microswitches. The other microswitches, with Au and binary alloy contacts, all failed due to stiction.

SECTION IV. Conclusion

The purpose of this work was to develop a new analytic contact resistance model for microswitches employing hemispherical-shaped upper contacts and sputtered contact metals, and to show the design, fabrication, and test results for microswitches with metal alloy electric contacts. Overall, the results show increased microswitch reliability in exchange for a small increase in contact resistance for devices with bimetallic, binary alloy, and ternary alloy electric contacts.

ACKNOWLEDGMENT

The authors would like to thank Dr. J. Albrecht, Dr. F. Shi, Captain L. Starman, Dr. K. Leedy, and Dr. J. Ebel, for their theory and design inputs and assistance with developing the fabrication process.

References

1. G. Rebeiz, RF MEMS Theory Design and Technology, New York:Wiley, 2003.

2. S. Bromley, B. Nelson, "Performance of Microcontacts Tested with a Novel MEMS Device", *Proc. 47th IEEE Holm Conf. Elect. Contacts*, pp. 122-127, 2001.

3. S. Majumder, "Study of contacts in an electrostactically actuated microswitch", *Sens. Act. A.*, vol. 93, no. 1, pp. 19-26, 2001.

4. G. Wexler, "The size effect and the nonlocal Boltzmann transport equation in orifice and disk geometry", *Proc. Phys. Soc.*, vol. 89, pp. 927-941, 1966.

5. R. Holm, Electric Contacts: Theory and Applications, Germany, Berlin:Springer, 1969.

6. W. Chang, I. Etison, D. Bogy, "An elastic-plastic model for the contact of rough surfaces", *ASME J. Tribol.*, vol. 109, pp. 257-263, 1987.

7. L. Kogut, K. Komvopolous, "Electrical contact resistance theory for conductive rough surfaces", *Amer. Inst. Phys.*, vol. 94, no. 5, pp. 3153-3162, 2003.
8. L. Kogut, K. Komvopolous, "Electrical contact resistance theory for conductive rough surfaces separated by a thin insulating film", *Amer. Inst. of Phys.*, vol. 95, no. 2, pp. 576-585, 2003.
9. W. Chang, "An elastic-plastic model for a rough surface with an ion-plated soft metallic coating", *J. Wear*, vol. 212, pp. 229-237, 1997.
10. A. Mikrajuddin, F. Shi, H. Kim, K. Okuyama, "Size-dependent electrical constriction resistance for contacts of arbitrary size: from Sharvin to Holm limits", *Proc. Mater. Sci. Sem.*, vol. 2, pp. 321-327, 1999.
11. D. Peroulis, S. Pacheco, K. Sarabandi, L. Katehi, "Electromechanical considerations in developing low-voltage RF MEMS switches", *IEEE Trans. Microw. Theory Tech.*, vol. 51, no. 1, pp. 259-70,, Jan. 2003.
12. S. Majumder, J. Lampen, R. Morrison, J. Maciel, "MEMS Switches", *IEEE Instrum. Meas. Mag.*, vol. 6, no. 1, pp. 12-15, Mar. 2003.
13. S. Duffy, "MEMS microswitches for reconfigurable microwave circuitry", *IEEE Microw. Wireless Compon. Lett.*, vol. 11, no. 3, pp. 106-108, Mar. 2001.
14. J. Schimkat, "Contact measurements providing basic design data for microrelay actuators", *Sens. Act. A.*, vol. 73, pp. 138-143, 1999.
15. P. Zavracky, S. Majumder, N. McGruer, "Micromechanical switches fabricated using nickel surface micromachining", *J. MEMS*, vol. 6, no. 1, pp. 3-9, 1997.
16. E. Abbot, F. Firestone, "Specifying surface quantity - a method based on the accurate measurement and comparison", *ASME Mech. Eng.*, vol. 55, pp. 569, 1933.
17. C. Calladine, Plasticity for Engineers, U.K., Chichester:Ellis Horwood, 1985.
18. L. Kogut, I. Etsion, "Elastic Plastic Contact Analysis of a Sphere and a Rigid Flat", *J. Appl. Mech.*, vol. 69, pp. 657-662, 2002.
19. J. Greenwood, J. Williamson, "Contact of nominally flat surfaces", *Proc. Royal Soc. A.*, vol. 295, pp. 257-263, 1966.
20. J. McCool, "Predicting microfracture in ceramics via a microcontact model", *ASME J. Tribol.*, vol. 108, pp. 380-386, 1986.
21. J. Greenwood, J. Tripp, "The contact of two nominally flat rough surfaces", *Proc. Inst. Mech. Eng.*, vol. 185, pp. 625-633, 1971.
22. N. Agraït (Agrait), "Quantum properties of atomic-sized conductors", *Phys. Rep.*, vol. 377, pp. 81-279, 2003.
23. G. Kovacs, Micromachined Transducers Sourcebook, New York:McGraw-Hill, 1998.
24. J. Shigley, C. Mischke, Mechanical Engineering Design, New York:McGraw-Hill, 1990.
25. M. Madou, Fundamentals of Microfabrication, FL, Boca Raton:CRC Press, 2002.
26. 2003, [online] Available: .
27. D. Hyman, M. Mehregany, "Contact physics of gold microcontacts for MEMS microswitches", *IEEE Trans. Compon. Packag. Technol.*, vol. 22, no. 3, pp. 357-64, Sep. 1992.
28. H. Okamato, Binary Alloy Phase Diagrams, OH, Materials Park:ASM International, 1992.